TUNNEL JUNCTION FORMATION ON SILICON P++ EMITTERS BY GAS IMMERSION LASER DOPING

G. Gaspar[1*], A. Guerra[1], F. C. Serra[1], A. S. Viana[2], J. Arumughan[3], I. Costa[1], D. M Pêra[1], J. A. Silva[1], L. Vines[4], J. M. Serra[1], K. Lobato[1]
[1]Instituto Dom Luiz (IDL), Faculdade de Ciências, Universidade de Lisboa, 1749-016, Lisboa, Portugal
[2]Centro de Química Estrutural, Faculdade de Ciências (CQE), Universidade de Lisboa, 1749-016, Lisboa, Portugal
[3]International Solar Energy Research Center (ISC), D-78467 Konstanz, Germany
[4]Department of Physics, Center for Materials Science and Nanotechnology, University of Oslo, N-0316 Oslo, Norway
*e-mail: gmgaspar@fc.ul.pt

ABSTRACT: Monolithically integrated 2-terminal Si/perovskite tandem solar cells have the potential to overcome the efficiency of Si single junction devices, whilst being cost-effective. The formation of the layers interconnecting the two sub-cells is a critical step, with several possible pathways for monolithic integration, such as amorphous Si, TCOs and crystalline silicon tunnel junctions. The latter one has the advantage of transparency, whilst also being more stable under high temperature steps required to deposit the perovskite sub-cell over the silicon sub-cell.
Here we report on the status of our approach at forming tunnel junctions directly on a silicon sub-cell using Gas Immersion Laser Doping (GILD). We believe that this approach is scalable, cost-effective, and simple to integrate into manufacturing lines, unlike tunnel junction formation by eg, ion implantation. Our GILD system has already been used to successfully form phosphorus doped thin (100 to 400 nm) layers on p-type Cz-Si wafers.
We now present the results of laser processing dependence according to wafer type (p^{++} emitter on p^{+} Cz-Si wafer vs p-type Cz-Si wafer without an emitter) and surrounding atmosphere. These influence the resultant surface morphology and the boron/oxygen depth profiles.
Keywords: Tandem Solar Cells; c-Si Tunnel Junction; Laser Doping

1 INTRODUCTION

On monolithically integrated 2-terminal Si/perovskite tandem solar cells, interconnecting the two sub-cells is a critical step that will impact the quality of the final device, since this layer must: (i) efficiently transport each sub-cell carrier types; (ii) have a high vertical conductivity, but low lateral conductivity; and (iii) be optically transparent (low absorption and reflectivity). Several approaches to produce the interconnecting layer have been developed such as amorphous Si (a-Si), transparent conducting oxides (TCOs) and crystalline silicon tunnel junctions [1,2].

An a-Si layer on top of the Si sub-cell restricts the fabrication of the top-cell layers to low temperature processing techniques (below 200 ºC) since degradation of a-Si will occur above this temperature [3].

Common TCOs like indium zinc oxide (IZO) and indium tin oxide (ITO), have successfully been used as a recombination layer between the two sub-cells. Lab-scale solar cells using indium zinc oxide (IZO) and indium tin oxide (ITO), achieved power conversion efficiencies of 19.2% and 25.1%, respectively [4, 5]. Despite having good electro-optical properties, these oxides have indium, a rare earth metal, which might impact on future widespread TW PV deployment.

Crystalline silicon tunnel junctions are formed by joining two highly doped layers n^{++}/p^{++}, as the abrupt shift in the band diagram (valence and conduction bands aligned) allows for the electron tunnelling effect between these two layers, without energy loss.

Plasma-enhanced chemical vapor deposition (PECVD) has been used to create nanocrystalline silicon tunnel junctions on top of the silicon heterojunction sub-cell, followed by the formation of the perovskite top-cell, yielding a 25.2% power conversion efficiency device [6]. Silicon tunnel junction have also been produced by ion implantation and crystalline silicon sub-cell devices [7].

We believe that Gas Immersion Laser Doping (GILD) [8] is also a viable option to create a silicon tunnel junction, and unlike the two previously mentioned techniques, it is scalable, cost-effective, and easier to integrate into manufacturing lines. The GILD process consists in the main following steps: (i) sample is immersed in atmosphere containing dopant source; (ii) shallow surface melting occurs by laser pulsing; (iii) surface adsorbed dopant is dissolved into the melt and rapidly diffuses within melt region; (iv) melt recrystallizes; (v) dopant surface re-adsorption; and (vi) melting of adjacent region by another laser pulse.

Previously, we successfully shallow doped p-type Cz-Si wafers with phosphorus at atmospheric pressure, using the GILD technique. Morphological analysis of the processed Si revealed shallow melting of the surface with the formation of pyramidal-like structures. Secondary ion mass spectrometry (SIMS) depth profiling showed phosphorus incorporation into Si, with doping depth and concentration profile depending on laser processing parameters [9].

In this paper, we present the results delivered by our GILD setup for a different silicon wafer, a p^{+} Cz-Si wafer with a highly doped p^{++} emitter on top. Field-emission scanning electron microscopy (FE-SEM) and SIMS show that both atmosphere chemical composition and wafer type have an impact on the laser processed sample properties.

2 EXPERIMENTAL

The experimental setup comprises two main systems, the reaction chamber, and the laser apparatus. It is described in detail elsewhere [9].

A cylindrical reaction chamber (see Fig. 1), made in aluminum with an IR-transparent window, can hold up to 10 x 10 cm^2 silicon wafers. The chamber is connected to a gas feed system, capable of delivering both argon and $POCl_3$ through a bubbler containing the liquid phosphorus precursor [10,11].

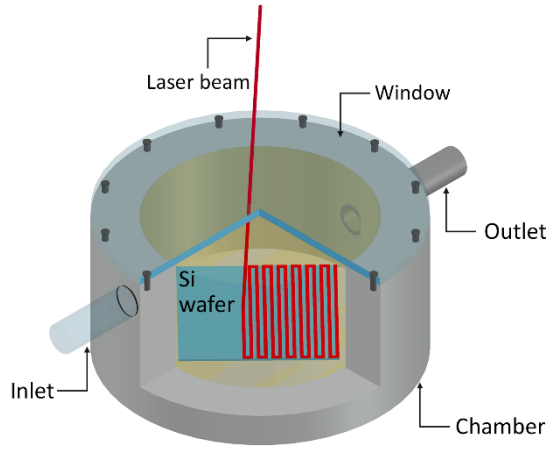

Figure 1: Reaction chamber schematic. A Si wafer placed in a $POCl_3$-rich atmosphere is laser processed.

After placing the silicon wafer and closing the chamber with the window, a series of vacuum and argon filling cycles were performed. Then, with the chamber's inner pressure set, an argon flow at 1.05 bar, passing through the $POCl_3$ bubbling system was maintained until the reaction chamber pressure equals, saturating its atmosphere with $POCl_3$ (vapor partial pressure of 0.037 bar at 293 K [12,13]).

Surface melting of the Si wafer was accomplished by laser rastering sequences with a 1064 nm solid-state pumped laser. Laser properties, such as pulse energy (0.04 mJ), pulse rate (500 kHz), beam diameter (20 µm) and distance between scan lines (10 µm), were kept constant. Laser rastering parameters, such as distance between consecutive laser spots (d = 1.0, 1.5, 2.0, 2.5 and 3.0 µm) and number of rastering sequences (n = 1, 3, 6, 9 times) were varied and combined to obtain a wide range of 10 × 5 mm^2 laser processed areas with different surface morphologies and doping depth profiles. Fig. 2 summarizes the process flow of the laser doping setup.

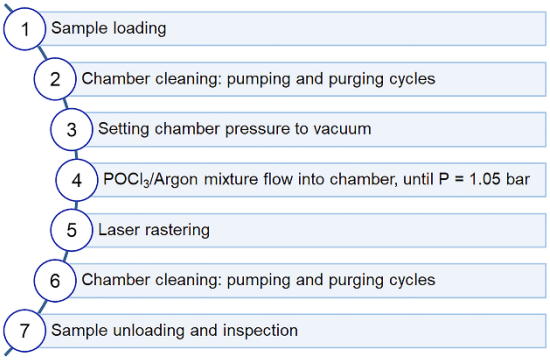

Figure 2: Summarized process flow diagram of the laser doping setup.

p^+ (100-oriented) Cz-Si wafers with a p^{++} emitter were used. The wafers are 100 mm in diameter, 525 µm thick, the base dopant concentration is ~ 10^{16} - 10^{17} cm^{-3} and the emitter side is mirror-like mechanically polished. Emitter peak surface dopant concentration and emitter depth are ~ 10^{20} cm^{-3} and ~ 0.4 µm, respectively, and were produced through a standard boron diffusion in a tube furnace apparatus.

3 RESULTS AND DISCUSSION

3.1 Surface morphology

Wafer type influences the surface morphology of the laser processed samples, as seen in FE-SEM micrographs of Fig. 3. Both p-type Cz-Si wafers and p^{++} emitter on p^+ Cz-Si wafers were laser processed.

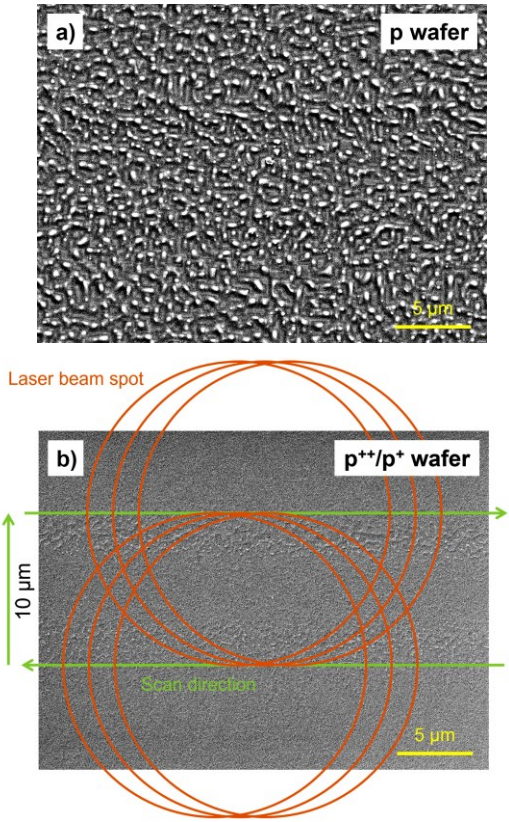

Figure 3: High-resolution FE-SEM micrographs (4000× magnification) of laser processed samples under argon atmosphere, using d = 2 µm, n = 1×: a) p-type Cz-Si wafer; b) p^{++} emitter on p^+ Cz-Si wafer.

The p-type Cz-Si wafer has a surface with a high density of pyramidal-like shape structures with sharp edges and sub-µm size bases, an indication of facet growth mechanism during melt recrystallization. It should be pointed out that while the structure base edges are in the sub-µm size range, their heights are in the 10-100 nm size range [9].

The p^{++} emitter on p^+ Cz-Si wafer has a smoother surface morphology, with both lower density and sized structures. This allows us to visualize the interaction of the successive laser pulses on the sample's surface. As the laser pulse moves in the direction marked by the superimposed green arrows, the rear part of the laser pulse creates consecutive circular recrystallized crusts separated by ca 2 µm (the distance between consecutive laser spots, marked as orange circles). The distance between scan lines is 10 µm, thus the next scan line above the previous one, remelts half the recrystallized surface below the center of the current laser pulse, leaving behind the same consecutive circular pattern, but in the opposite direction. It is also clearly noticeable the formation of structures at the edge of each scanned line distancing apart ca 10 µm. It is possible that these structures are formed as molten silicon is released from the laser spot due to Marangoni

forces present in the molten areas [14].

The difference in surface morphology between the p-type Cz-Si wafer and p^{++} emitter on p^{+} Cz-Si wafer is clear evidence of higher laser interaction on the p-type Cz-Si wafer. This may be attributed to the following factors: (i) lower thickness (275 µm), of the p-type Cz-Si wafer, thus heat loss rate by conductivity is lower; (ii) lower boron doping level of the p-type Cz-Si wafer, 10^{15} cm^{-3}; and (iii) different surface reflectivity.

Fig. 4 presents the FE-SEM micrographs of the p^{++} emitter on p^{+} Cz-Si wafer. Samples were laser processed by varying the number of rastering sequences, with both sets processed under argon or $POCl_3$ atmospheres respectively.

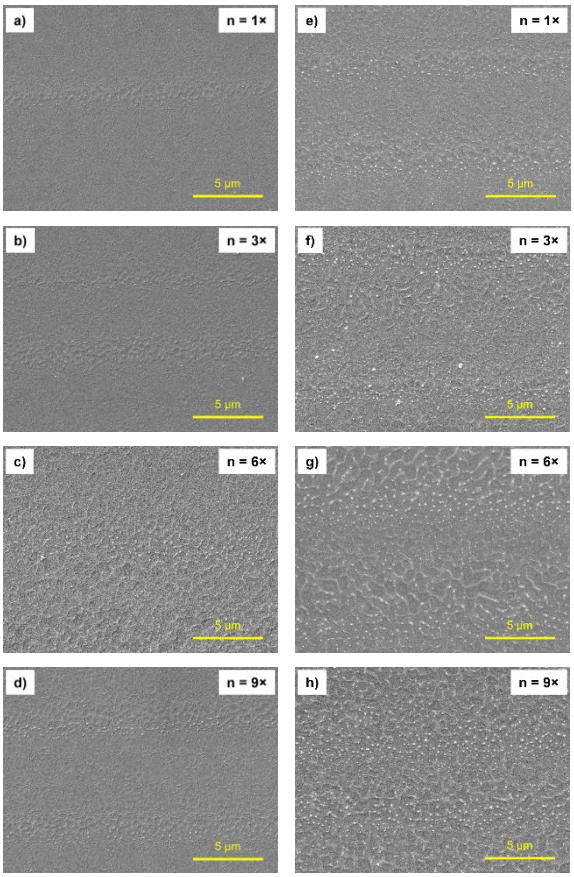

Figure 4: High-resolution FE-SEM micrographs (4000× magnification) of laser processed samples using a fixed laser spot spacing of d = 2 µm and varying number of rastering sequences (n = 1×, 3×, 6×, 9×). Comparison between argon, a) to d), and $POCl_3$, e) to h), atmospheres.

Under argon atmosphere there is a noticeable increase in structure size and density on the sample's surface as the number of rastering sequences increases from 1 to 9. The same behavior is also present on the samples processed under $POCl_3$ atmosphere, with the increase of laser interaction resulting in a rougher surface morphology. For the same number of rastering sequences, samples processed under $POCl_3$ atmosphere always showed higher surface roughness than the equivalent argon processed sample. Adsorbed $POCl_3$ plays a key role in increasing the laser interaction.

3.2 Boron and oxygen depth profiles

Boron and oxygen depth profile concentrations of p^{++} emitter on p^{+} Cz-Si wafer laser processed samples under argon atmosphere were measured with SIMS using a Cs primary ion beam at 15 keV to sputter craters of 100 × 100 $µm^2$ and obtaining data from a physical aperture of 8 µm diameter. Boron depth profile concentrations are shown in Fig. 5.

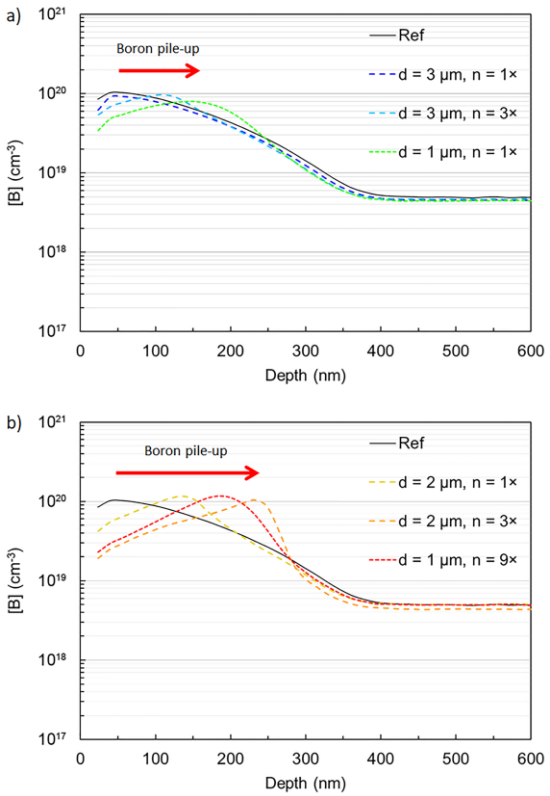

Figure 5: SIMS boron depth profiles for unprocessed reference sample (black solid line), and processed ones under argon atmosphere using: a) lower laser interaction conditions (d = 3 µm, n = 1×; d = 3 µm, n = 3× and d = 1 µm, n = 1×); b) higher laser interaction conditions (d = 2 µm, n = 1×; d = 2 µm, n = 3× and d = 1 µm, n = 9×).

Samples processed with lower laser interaction conditions show a small yet noticeable increase of boron concentration towards the maximum melt depth (taken as the point where the concentration profile matches the Ref), whilst there is also a decrease in concentration closer to the sample surface. This effect is more pronounced in samples processed with higher laser interaction conditions with a distinct "shoulder" becoming apparent.

This phenomenon, known as boron-pile up at maximum melt depth, is due to the segregation coefficient for boron being greater than 1 when high recrystallization velocities are present, as is the case here. As opposed to steady state melt conditions, where the boron segregation coefficient is 0.8 causing segregation of boron into the melt, a higher than 1 value causes the boron to pile-up at greater depths where the silicon begins to recrystallize [15].

Oxygen depth profile concentrations are shown in Fig. 6.

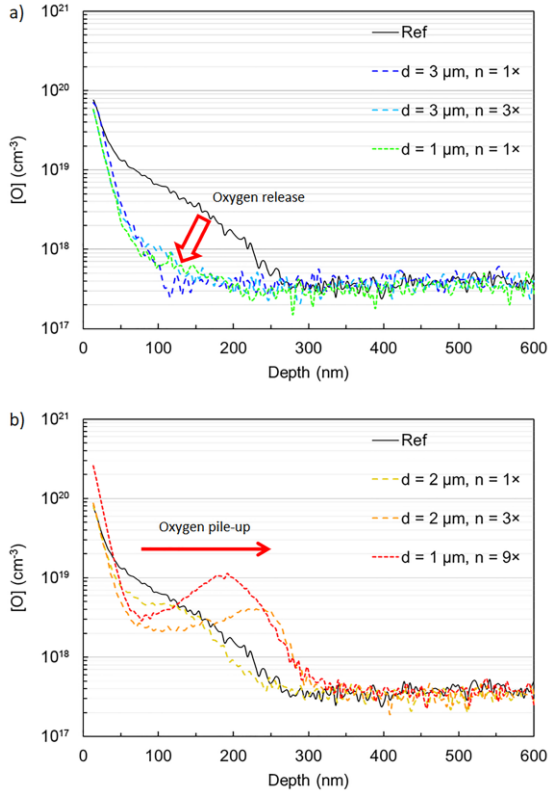

Figure 6: SIMS oxygen depth profiles for unprocessed reference sample (black solid line), and processed ones under argon atmosphere, using: a) lower laser interaction conditions (d = 3 µm, n = 1×; d = 3 µm, n = 3× and d = 1 µm, n = 1×); b) higher laser interaction conditions (d = 2 µm, n = 1×; d = 2 µm, n = 3× and d = 1 µm, n = 9×). Nb: the apparent oxygen concentration of ca. 4×10^{17}cm^{-3} is due to the limits of the SIMS system (eg, O_2 gas entering the vacuum chamber) and do not represent the true bulk oxygen content.

Samples processed with lower laser interaction conditions present a decrease in oxygen concentration. The oxygen, due to its high vapor pressure, evaporates from the molten silicon as SiO gas before the rapid recrystallization [16].

Oxygen pile-up occurs when the sample is processed with higher laser interaction conditions, as also observed for boron. This is in-line with the oxygen segregation coefficient being greater than 1 under these rapid recrystallization conditions [17]. However, oxygen concentration remains high at the surface. The maximum melt depths (taken as where the concentration profile returns to the Ref baseline), are in line with those inferred from the boron concentration profiles.

4 CONCLUSIONS

The experimental setup has proven effective in surface shallow melting of p^{++} emitter on p^{+} Cz-Si wafers, in a $POCl_3$ environment at atmospheric pressure.

Wafer surface doping level influences laser interaction, as laser interaction is weaker with higher doping level.

For p^{++} emitter on p^{+} Cz-Si wafers we observe: (i) increasing the number of rastering sequences results in greater laser interaction, as SEM micrographs show rougher surface morphology; and (ii) addition of $POCl_3$ doping atmosphere results in higher surface roughness.

SIMS depth profiles of p^{++} emitter on p^{+} Cz-Si wafer show: (i) for boron, a distinct "shoulder" appears as the laser interaction is more intense (boron pile-up towards the maximum melt depth [5]); and (ii) oxygen is released for low laser interaction, whilst pile-up occurs for higher laser interaction, representing segregation into the bulk.

REFERENCES

[1] M. Jošt *et al.*, Advanced Energy Materials 10 (2020) 1904102.
[2] Y. Ko *et al.*, Advanced Materials 32 (2020) 2002196.
[3] S. Albrecht *et al.*, Energy & Environmental Science 9 (2016) 81.
[4] J. Werner *et al.*, The Journal of Physical Chemistry Letters 7 (2016), 161.
[5] P. Schulze *et al.*, Solar RRL 4 (2020) 2000152.
[6] F. Sahli *et al.*, Nature Materials 17 (2018) 820.
[7] P. Bellanger *et al.*, IEEE Journal of Photovoltaics 8 (2018) 1436.
[8] G. B. Turner *et al.*, Applied Physics Letters 39 (1981) 967.
[9] G. Gaspar *et al.*, Proceedings 37th European Photovoltaic Solar Energy Conference (2020) 765.
[10] H. Li *et al.*, Frontiers in Energy 11 (2017) 42.
[11] H. Ghembaza *et al.,* Silicon 10 (2018) 377.
[12] D. R. Stull, Industrial & Engineering Chemistry 39 (1947) 518.
[13] National Institute of Standards and Technology, NIST Chemistry WebBook, SRD 69 (2021, September 8).
[14] E. Haro-Poniatowski *et al.,* Journal of Applied Physics 115 (2014) 224309
[15] P. C. Lill *et al.*, Materials 10 (2017) 189.
[16] G. Gaspar *et al.*, Journal of Crystal Growth 418 (2015) 176.
[17] M. Ametowobla, Characterization of a laser doping process for crystalline silicon solar cells, PhD Thesis, University of Stuttgart (2010).

ACKNOWLEDGEMENTS

This work was supported by the S-LoTTuSS project through the grant agreement PTDC/CTM-CTM/28962/2017, financed by national funds FCT/MCTES (PIDDAC), and by FCT – Project UIDB/50019/2020 – IDL – Instituto Dom Luiz.
The authors acknowledge the support from The Research Council of Norway (RCN) through Project No. 239895/F20.